Proposal of Bond Behavior Simulation Model by Using Discretized Voronoi Mesh for Concrete and Beam Element for Reinforcement

Usman Farooq*, Hikaru Nakamura, Taito Miura, Yoshihito Yamamoto

Department of Civil and Environmental Engineering, Nagoya University, Furo-cho, Chikusa-ku, Nagoya, 464-8603, Japan

*Corresponding Author

Email Address: u.farooq1710@gmail.com (U. Farooq), hikaru@cc.nagoya-u.ac.jp (H. Nakamura), t.miura@civil.nagoya-u.ac.jp (T. Miura), y.yamamoto@civil.nagoya-u.ac.jp (Y. Yamamoto)

Abstract

This study proposed an analytical method based on the Three Dimensional Rigid Body Spring Model (3D-RBSM) to realistically simulate bond behavior of deformed rebar in concrete. In this method, concrete was modeled by rigid particles using a voronoi mesh with random geometry and rebar was modeled by beam element connected to concrete through a link element that was assigned a suitable local bond model. The proposed model enables to evaluate changes in internal cracking and stress distribution due to variation in cover thickness and rebar diameter. Furthermore, it can simulate the bond stress slip behavior and transition of failure modes. Based on analytical results, it was confirmed that the proposed simplified model can evaluate bond behavior like three dimensional rebar model with rib shape, consequently, it provides an economical and efficient alternative due to lesser computational elements.

Keywords: Bond Behavior, 3D-RBSM, Voronoi Mesh, Beam Element, Concrete Cover, Rebar Diameter

Highlights

- A simplified bond model based on 3D-RBSM is proposed by using voronoi mesh for concrete and beam element for reinforcement to evaluate bond behaviors.
- A CEB-Shima hybrid local bond model is proposed and utilized in 3D-RBSM to simulate bond behavior, reasonably.
- Voronoi mesh has a vital role to simulate bond behavior and crack distribution by using a beam element model for 3D-RBSM.
- The simplified bond model can evaluate the effect of structural parameters such as concrete cover thickness and rebar diameter on bond stress slip relationship and crack and stress distribution mechanism.

1. Introduction

Bond interaction between reinforcement and concrete is one of the most important characteristics of reinforced concrete members. Several experimental studies [1-4] have been conducted since the 1910s to understand the fundamental differences of bond mechanism between deformed and round rebar in concrete. Whereas, it was highlighted that for deformed rebar, bearing stresses due to the interlocking of concrete between ribs had a significant influence on the bond behavior as compared to the frictional and adhesion stresses being the only contributors for the round rebar. Furthermore, Broms et al. [5] and Goto [6] used special coloring techniques injected into the pullout specimen to visualize and understand the bond mechanism of internal cracks near to the ribs of deformed rebar. In these research themes, it was understood that interlocking of concrete between ribs is not the only sole contribution of deformed rebar to bond behavior, but the internal conical cracks formed at 45-60° angle (Fig. 1) also play a vital role in the bond mechanism of RC structure due to the formation of compression struts.

Bond behavior has a significant effect on the mechanical aspects of RC structures such as flexural and shear capacities, cracking behavior, hysteretic behavior, etc. However, it is a very complicated phenomenon being dependent upon several structural parameters. Numerous experimental researches [7-22] are performed on bond evaluation considering the influence of concrete strength, concrete cover, rebar diameter, stirrup ratio, embedment length, rib spacing, etc. In particular, Iizuka et al. [20] conducted research on the effect of variation in cover thickness on bond behavior based on a two-end pullout experiment. Results outlined an overall positive effect of the increase in cover thickness on bond behavior. Also, other researches on the effect of confinement [11, 18, 19 and 22] due to cover thickness or stirrup ratio expressed a gradual transition of failure mode from splitting to pullout failure with the increase in confinement level, so bond stresses increased significantly as well. Based on these studies, generalized local bond stress slip equations have been included in the design codes [23-25]. Particularly, CEB-FIP code [23] defines the effect of various structural parameters (concrete cover, stirrup ratio, etc.) in terms of confinement on bond behavior as shown in Fig. 2. Where the structural parameters are included as modification factors in the local bond stress slip equation.

In several finite element method (FEM) tools, non-linear bond slip behavior had been neglected by considering a perfect bond condition in case of smeared or embedded reinforcement modeling [26-28]. However, it had been often realized that prefect bond assumption results in over-estimation of experimental results [29], especially when a bond failure is expected to occur. For the better analytical evaluation of RC structures based on steel-concrete bond characteristics, non-linear bond stress slip modeling has been occasionally performed by several researchers [20, 30-32]. Where a discrete beam element model has been used considering a bond interface. In the beam element model, Gan [31] used several local bond models to simulate bond behavior for various RC members. Local bond models had a functional dependency on cover thickness, rebar diameter, confinement pressure, etc. Also, Lowes et al. [32] modeled a bond element of finite length between rebar and concrete element. Bond element had a rigorous dependency on several parameters including lateral pressure, rebar diameter, concrete cover, etc. It builds an understanding that discrete bond modeling in FEM is highly parametric dependent. Whereas the numerical outcomes are susceptible to incorrect estimations due to variation in structural parameters and bond conditions, and test data being limited. Moreover, it should be noted that bond behavior is evaluated without the representation of the internal cracks as observed in Goto's study that is an essential phenomenon of deformed rebar structures [5, 6]. To overcome these disadvantages, a mesoscale based 3D rebar model with rib shape (3D model) is applied as an alternative methodology of the beam element model (beam model).

In FEM, by utilizing a 3D model in the combination of a smeared crack model, bond behavior along the internal cracking mechanism can be simulated. Salem et al. [33] used a 3D model to simulate pre and post-yield bond behavior. While Kurumatani et al. [34] used this model to simulate internal cracking behavior and the overall effect of different chloride concentrations on damage evaluation of RC members. Recently, several researchers are using a discrete element based Three Dimensional Rigid Body Spring Model (3D-RBSM) that enables to directly evaluate the crack propagation process. In 3D-RBSM, Eddy et al. [35] simulated the influence of stirrups on bond behavior for a beam-column joint by using the 3D model and showed the applicability of this method to evaluate the effect of confinement levels on bond related mechanical properties. Also, by using the model in 3D-RBSM, Ikuma et al. [36] simulated the effect of cover thickness on bond behavior. However, the bond evaluation aspect of the 3D model has several computational disadvantages. It requires a very fine mesh size for concrete [34-36] in the vicinity of rebar to evaluate the influence of the rib on bond behavior. Also, a considerable number of mesh elements are required for reinforcement itself. Due to this, computational elements are compelled to exponentially increase. Hence, it suffers through huge computational cost and time. Most importantly, the 3D model is applicable for only a small scale of members due to the limited computational capacity in the present era.

The objective of the present study is to validate the utilization of beam model for reproducing signature bond behaviors of reinforced concrete using 3D-RBSM. In this proposed model, the link element introduced by the local bond model was applied to connect the beam element of rebar to the voronoi element of concrete. The local bond model is parametrically independent, unlike FEM. With the proposed simplified model, the influence of variation in concrete cover thickness on bond stress slip relationship and crack propagation was evaluated similarly to a 3D model. The effect of variation in rebar diameter on the bond behavior was also simulated. Furthermore, the stress distribution mechanism of bond was explained based on variation in concrete cover thickness and rebar diameter.

2. Overview of 3D-RBSM

3D-RBSM is one of the discrete models. In RBSM, concrete is modeled as an assemblage of rigid particles interconnected by the springs arranged at their interfaces (Fig.3). The crack pattern is strongly affected by the mesh design since cracks initiate and propagate through the interface of particles. Therefore, a random geometry of rigid particles is generated by voronoi tesselation to reduce mesh bias on the initiation and propagation path of the cracks. Each rigid particle has three translational and three rotational degrees of freedoms defined at the center of gravity. The interface between two particles is divided into triangles with centroids and vertices of the surface. One normal and two shear springs are set at the center of each triangle.

The concrete constitutive models for tension and compression of normal springs and shear springs used in RBSM for monotonic loading analysis are constructed by uniaxial relationships between stress and strain, as shown in Figs. 4-8. The details of the models and the relevant model parameters have been described and verified in the research conducted by Yamamoto et al. [37, 38, 40].

Steel reinforcement is modeled as a series of regular beam elements [38] as shown in Fig. 9. In this model, the reinforcement can be freely arranged within the member domain, regardless of the mesh arrangement of concrete [39]. At each beam node, two translational and one rotational degree of freedom are defined employing the springs. The reinforcement is attached to concrete particles by zero-size link elements that are attached between beam node and particle computational point to provide a stress transfer mechanism between rebar and concrete. The distance between two link elements is similar to the rigid particle size of concrete. Each link element consists of tangential, normal and rotational springs around the rebar axis. Tangential spring is used to represent shear stress transfer due to the ribs and assigned a non-linear bond stress slip relationship. Normal spring is assigned very large stiffness to prevent displacement in the direction normal to the rebar [38]. The analytical method has been applied to many structural and durability problems such as flexural and shear failures under monotonic and cyclic loadings [40-42] and internal crack propagation due to rebar corrosion [43-45].

3. Beam Element based Reinforcement Model to Simulate Bond Behavior

3.1. Local Bond Stress Slip Models

Crack development is strongly dependent upon the bond interaction between concrete and reinforcement. The local bond stress-local slip relationships are indicated in Fig. 10 to make a comparison among several local bond models. Compressive strength and rebar diameter are set to 30MPa and 25.4mm, respectively. The green line shows the CEB-FIP local bond stress slip model [21]. This model is representative of pullout failure mode. Bond slip model has a dependency on concrete compressive strength, only. The constitutive law of the CEB-FIP model is shown in equation (1).

$$\tau = \tau_{max}(s/s_1)^{0.4} \quad s_1 \geq s \geq 0 \tag{1}$$

$$\tau_{max} = 2.5 \times {f'_c}^{0.5}$$

Where, τ: bond stress (MPa), f'c: compressive strength (MPa), s: slip (mm), while s_1: 1.0mm.

Shima et al. [12] formulated a bond model based upon the experimental outcomes of rebar embedded in massive size concrete specimens, a representation of a column-footing joint. To express the effect of various boundary conditions (long embedment, short embedment, uni-axial tension) on bond slip behavior, Shima et al. proposed a bond slip equation with the inclusion of rebar strain referred to as the bond-slip-strain relationship. However, considering a very long embedment length with the boundary condition of the slip being zero at a location where strain is zero and vice versa, the bond-slip-strain model was simplified as the bond slip model. This model is represented by the black line in Fig. 10. The constitutive relationship of the Shima local bond slip model can be seen in equation (2). Shima model has lower ultimate bond strength and rigid pre-peak stiffness as compared to CEB-FIP model. Also, the model has a functional dependency on rebar diameter and does not consider the post-peak softening behavior, unlike CEB-FIP model.

$$\tau = \tau_{max}(1 - \exp(-40(s/D)^{0.6}) \qquad s \geq 0 \tag{2}$$

$$\tau_{max} = 0.9 \times f'_c{}^{\frac{2}{3}}$$

Where, D: diameter of rebar (mm).

The blue line shows the model proposed by Suga et al. [46] that has been used to simulate several structural members in 3D-RBSM and FEM by Authors [38, 46]. The model was proposed by modifying the Shima model considering a strength reduction factor of ‘0.4’ and a power factor of ‘0.5’ for the structural analysis of RC members with a cover thickness smaller than massive concrete. Also, they proposed a softening curve to evaluate the post-peak behavior of RC members. For the case of the Suga model, the constitutive relationship of bond stress slip can be seen in equation (3).

$$\tau = \tau_{max}(1 - \exp(-40(s/D)^{0.5}) \qquad s_1 \geq s \geq 0 \tag{3}$$

$$\tau = \tau_{max} - (\tau_{max}(s - s_1)/(s_2 - s_1)) \qquad s_2 \geq s \geq s_1$$

$$\tau = 0.10 \times \tau_{max} \qquad s \geq s_2$$

$$\tau_{max} = 0.40\left(0.9 \times f'_c{}^{\frac{2}{3}}\right)$$

Where, s_1: 0.2 mm and s_2: 0.4 mm.

In this study, the authors present a new bond model based upon modification to the CEB-FIP model, termed as the “CEB-Shima hybrid” model. The objective of the model is to reasonably simulate the effect of various structural parameters on bond behavior, as will be illustrated in the next section. The proposed model is represented by the red line in Fig. 10. The initial loading stiffness of the model has a resemblance to the Shima model, being stiffer than the CEB-FIP model. In higher bond stress regions, ultimate bond stress and post-peak behavior are similar to the CEB-FIP model. For the proposed model, the modified constitutive function is given in equation (4). The simple modifications are suggested to the power factor being "1/3" besides "0.4" and the slip value (s_1) at ultimate bond stress being "0.9mm" besides "1.0mm".

$$\tau = \tau_{max}(s/s_1)^{1/3} \quad s_1 \geq s \geq 0 \tag{4}$$

$$\tau_{max} = 2.5 \times {f'_c}^{0.5}$$

3.2. Suitable Local Bond Model to Simulate Effect of Cover Thickness on Bond Behavior

Analytical outcomes of the before-mentioned local bond models are validated by two-end pullout experiments performed by Iizuka et al. [20]. The schematic diagram of the two-end pullout test can be seen in Fig. 11. In this experiment, the size of the specimen was 150mm cube. A rebar was embedded inside the specimen at the desired cover thickness and subjected to two-end pullout loading. While a strain gauge was installed on rebar at half of the embedment length to measure the strain to calculate the average bond stress. Also, LVDTs are used at both ends of the rebar to measure the average slip.

To compare several local bond models, three test specimens with a cover thickness of 10, 30 and 50mm are selected [20]. Rebar diameter and concrete strengths are 25.4mm and 25.1MPa, respectively. It is noted for the beam model that the cover thickness is equal to the summation of the actual cover thickness (C: 10, 30, or 50mm) and rebar radius (R) as shown in Fig. 12. An averaged mesh size of 10mm is throughout used to simulate the test specimens.

Fig. 13 presents a comparative study among several local bond models to evaluate the effect of cover thickness variation (10, 30, 50mm) on bond behavior. For the small cover thickness i.e. 10mm, all four models can reasonably predict experimental ultimate bond stresses. However, loading stiffness behavior varies for different local bond models. In the case of the Suga model, the stiffness is mildest as compared to all other local models as well as experiments. Also, the stiffness is milder for the CEB-FIP model than the experiments. On the other hand, the Shima model and CEB-Shima hybrid model can reasonably simulate experimental pre-peak stiffness behavior.

For the cover thickness of 30 and 50mm, the Suga model predicts constant bond stress slip behavior besides of increase in cover thickness and significantly underestimates experimental ultimate bond stresses due to the least local theoretical bond strength. Also, the predicted stiffness is considerably different in comparison to experiments. Suga model cannot evaluate the effect of an increase in cover thickness on elevated bond stresses in the objective experiment. On the contrary, for the case of the Shima model, CEB-FIP model, and CEB-Shima hybrid bond model, all three have the capability to reasonably estimate the increasing average bond stress of experiments with an increase in cover thickness. Regarding pre-peak behavior, the Shima model and CEB-Shima hybrid models show comparatively similar behavior to experiments than CEB-FIP due to higher initial stiffness of local bond models. The results of both models match reasonably with the experimental results in terms of pre-peak stiffness, peak bond stress, and slip at the peak bond stress. However, analytically evaluated post-peak behavior is different in comparison to experiments. These differences might be attributed to the significant experimental variation in the post-peak region. So, the analytical accuracy of the proposed model to simulate post-peak behavior is to be verified based on a broad range of two-end pullout test results along with various other experimental setups such as one-end pullout test, beam-end test, etc.

For all four local bond models, Figs. 14 and 15 illustrate the internal crack formation and the deformation pattern at 0.30mm slip to evaluate the influence of concrete cover thickness. The crack color gradient depends on the crack width. For the case of the Suga model, internal cracks don't propagate in the mid-section of the rebar and a split crack formation does not appear for each case of concrete cover thickness. Moreover, due to the low theoretical ultimate bond stress, the Suga model cannot reproduce the split crack formation. Formation of the split crack is a characteristic representation in pullout experimental studies for low to medium level confinements [5, 6, 18, 22]. On the other hand, CEB-Shima hybrid, CEB-FIP, and Shima models simulate an uneven distribution of the internal cracks along rebar length as observed in Fig. 14. Also, the formation of the split cracks at the surface of the specimen has appeared in Fig 15. Several experimental studies [18, 48, 49] had outlined that the bond stresses increase with increment of C/D ratio. This experimental observation has been simulated by all three local bond models, whereas the split crack formation tendency has reduced with an increase in cover thickness from 10 to 50mm, consequently, ultimate bond stresses increased.

CEB-Shima hybrid model and Shima model showed similar and reasonable results to simulate both bond slip and internal cracking behavior. However, certain drawbacks are associated with the Shima model. The model is based on long embedment length boundary condition, so the applicability to a wide range of boundary conditions (short embedment, uni-axial tension) is limited, particularly for the structural members with higher bond stresses as experimentally observed [11, 14, 21, 23]. Also, the model does not consider a post-peak softening behavior that is an important failure characteristic. In addition, it has a dependency upon rebar diameter. On the other hand, the utilization of the CEB-Shima hybrid model in 3D-RBSM can express the effect of various boundary conditions on bond behavior and a simplified bond stress slip approach is provided without rebar diameter. As the evaluated test specimens are subjected to split failure mode, so in present analytical evaluation, the target of authors is only the pre-peak modeling of CEB-Shima hybrid bond model. Considering these advantages, the CEB-Shima hybrid bond model is proposed as the bond model to be utilized in 3D-RBSM. So in the next sections, the CEB-Shima hybrid bond model will be utilized throughout to highlight the peculiar advantages of the proposed analytical method based on beam element and voronoi mesh.

Furthermore, the initiation and progression of cracks have been rarely outlined for a typical two-end pullout test with short embedment length as in the case of Iizuka et al [20]. So the crack formation process based on the proposed analytical method with the CEB-Shima hybrid bond model is shown in Fig. 16 for the specimen with 30mm cover thickness. Cracks are shown at the surface near to the minimum cover thickness at peak bond stress and in the post-peak stage at slip values of 0.15mm, 0.20mm, and 0.30mm. It is observed that just at peak bond stress, longitudinal crack progresses from the end of the rebar due to stress concentration in this region. Later on, as slip progresses into post-peak range then the longitudinal cracks branch into two cracks transverse to the rebar direction.

3.3. An Economical and Efficient Alternative of the Mesoscale 3D Rebar Model

As explained before, to simulate experimentally observed conical crack propagation from the rib surface of deformed rebar leading to the characteristic ring tension effect and realistic local bond behavior, several researchers have utilized a 3D rebar model [33-36]. On the other hand, it was shown in the previous section that the proposed model based on a simple beam element with the combination of voronoi mesh in 3D-RBSM can also simulate conical cracks propagation from the rib surface as well as experimentally observed bond stress slip behavior. In this section, to build a bond based on comparative study between 3D model and beam model of reinforcement, the results of simulated specimens in the previous section are compared with the results of Ikuma et al [36], who simulated same specimens by constructing 3D rebar model with rib shape in 3D-RBSM.

Comparative bond stress slip relationships are presented in Fig. 17. 3D rebar model illustrates an increase in the ultimate bond stresses and slips at ultimate bond stresses with an increase in cover thickness and also a change in the stress slip stiffness. Although, the 3D rebar model overestimated the bond strength of test results for smaller cover cases (10/30mm) and the beam element model underestimated the one for larger cover case (50mm). However, both models show sufficient accuracy to simulate bond stress slip behavior as observed in experiments, considering the pre-peak region. These observations confirmed the reasonableness and usefulness of the proposed beam element model. Although, the results of the proposed model show ductile behavior than test results in the post-peak region, however, 3D rebar model also showed the ductile behavior. The differences in the post-peak region should be discussed not only based on the proposed beam element model but also based on the 3D rebar model along with variation in test results, considering a broad range of two-end pullout tests along with various other experimental setups such as one-end pullout test, beam-end test, etc.

Fig. 18 shows the comparison of deformation behavior, internal crack propagation and cracking pattern near rebar interface at a slip value of 0.15 and 0.30mm for the 30mm cover case. The internal crack formation gives a visualization of crack width as shown by the color gradient. The range of simulated crack width as well as the pattern is similar for both models. With both models, internal cracks progressed at 45-60° angle to the rebar axis that is a consistent cracking mechanism in comparison to the Goto's study as shown in Fig. 1. According to the deformation diagram, the propagation of split cracks in the longitudinal and transverse direction of rebar is observed in the case of the 3D model. Also, in the case of the beam element model, the formation of the same split cracks can be confirmed. Goto's study explained that inclined formation (45-60° angle) of internal cracks in the vicinity of rebar causes the propagation of longitudinal split cracks in the direction of rebar. This mechanism has been well simulated with the beam model and the 3D model. Overall, results indicate that the beam model and 3D model can simulate the effect of cover thickness on local bond characteristics.

It is an important fact that the 3D model has several computational drawbacks. To simulate a specimen of 150mm cube size merely, the 3D model requires 24,000 elements approximately. Moreover, rebar has to be arranged at locations with very fine mesh and modeling of ribs requires particular attention that can be a hindrance for member level evaluation considering multi-dimensional reinforcement arrangement. These are computationally inefficient and uneconomical aspects of the 3D model. While, with the beam model, modeling of the same size specimen requires 2500 elements only based on a 10mm mesh size that is ninth times lesser than the 3D rebar model. Moreover, the rebar model based on beam element can be freely arranged in specimen domain rendering ease to the user for multi-dimensional reinforcement arrangement. It is proven that the proposed model is a good numerical substitute of the 3D model with efficient and economical aspects and applies to a wide range of structural members.

3.4. Mesh Size and Discretization Dependency

Random geometry of rigid particles slightly shows mesh arrangement differences and mesh size dependency. Moreover, the distance between two link elements to provide shear force transmission between rebar and concrete depends on rigid particle size. Therefore, mesh size dependency is necessary to be verified. To do so, mesh sizes of 5, 10, 15, and 30mm are selected as shown in Fig. 19 along with the number of elements for respective cases. Also, to verify the mesh discretization effect, 15mm mesh size case is re-meshed, so two cases as 15mm-1 and 15mm-2 are considered as shown in Fig. 19. It should be noted that the computational time can be significantly decreased with an exponential decrease in computational elements. Fig. 20 represents the influence of mesh size on bond stress slip behavior for test specimen of 30mm concrete cover, 25.4mm rebar diameter, and 25.1MPa concrete strength. It shows that ultimate bond stresses and pre-peak stiffness increase slightly and post-peak behavior become ductile with an increase in mesh size from 5 to 30mm. Also, it can be seen that the mesh discretization based on 15mm mesh size has a negligible effect on bond stress slip behavior.

The internal cracking pattern at 0.30mm slip can be seen in Fig. 21. With an increase in mesh size, the internal cracking intensity reduces because of mesh size approaching to cover thickness, so there is a slight increase in bond stresses and stiffness gradient. Overall, analytical results with a mesh size of 5 to 30mm can reasonably predict the experimental results. If the mesh size is smaller than the cover thickness, the proposed model is appropriately applicable to simulate bond behavior with the internal cracking pattern. Utilization of the mesh size in the range close to cover thickness provides an economical and efficient tool for the evaluation of large size concrete structures. Furthermore, with mesh discretization, there is no significant effect on the internal cracking behavior.

4. Dominant Effect of Random Geometry of Voronoi Mesh to Simulate Bond Behavior with Beam Model

In several structural evaluation software based on FEM, a regular mesh shape is used for the modeling of concrete. While the irregular shape of voronoi mesh in 3D-RBSM is a characteristic representation of the concrete matrix. It is a sole element to reproduce realistic cracking mechanism in comparison to experiments. To understand the inherited ability of the beam model to simulate bond behavior based on the role of random geometry of voronoi mesh, a specimen with cubic shape regular mesh was modeled in 3D-RBSM as shown in Fig. 22. The size of the mesh is 10mm. Bond stress slip comparison between regular and voronoi mesh is built based on the same specimens as in chapter 3. For both types of mesh shapes, CEB-Shima hybrid model was used for the modeling of shear stress transfer (bond stresses) between rebar and concrete.

In Fig. 23, bond behavior comparison between regular and voronoi mesh with beam element is shown. Though the initial stiffness behavior until the initiation of the cracking is similar for both models, however, the ultimate bond stresses in the case of regular mesh are significantly lower than the experiments. It should be noted for regular mesh that overall bond stress slip behavior remains constant besides an increase in cover thickness. Hence, regular mesh with beam model cannot evaluate the effect of confinement on bond behavior, unless a bond model including the effect of cover thickness is utilized. This fact has also been recognized in researches based on FEM [20, 31, 32]. In case of beam element model with voronoi mesh-based irregular shape, the effect of confinement on bond behavior can be reasonably evaluated, while the bond model does not need to consider several structural aspects as modification factors in bond stress slip equation as like FEM.

Fig. 24 shows crack pattern at rebar interface for regular mesh considering all three cover thickness cases at 0.15 and 0.30mm slip. The distribution of internal cracks always follows the boundary of mesh shape. In the case of regular mesh, internal cracks progressed at 90° angle to the rebar axis with shear transfer action. The formation of internal cracks is different in comparison to the Goto's study as shown in Fig. 1. Hence, regular mesh shape is incapable to simulate the actual internal cracking mechanism of deformed rebar structures. Also, transverse split cracking at the surface of the concrete is not simulated with regular mesh shape.

To illustrate the sole reason behind entirely different cracking pattern and bond stress slip behavior between regular and voronoi mesh, Fig. 25 shows the mechanism of stress transfer from shear spring in rebar direction along with internal stress distribution. As for the beam element model, a link element with tangential (shear) spring is used to transfer the shear stresses. So, when a regular mesh is used, shear stresses from the beam element cannot completely transfer to the outer region of concrete and remain localized in the vicinity of the rebar. A regular mesh doesn't simulate the conical stress distribution phenomenon. Hence the entire concrete section cannot be effective to resist shear stresses originated from the beam element. Stress localization causes the localization of cracks in the surrounding of rebar. Overall, the bond stresses remain lower than the experiments. On the other hand, with the irregular shape of voronoi mesh, propagation of tensile stresses away from reinforcement in the form of ring-tension can be observed. Most importantly, the formation of compression struts in the vicinity of the beam element is observed. These compression struts produce due to the formation of conical cracks that is an actual bond mechanism observed in Goto's study [6]. Simulation of ring-tension and compression struts reflects experimentally observed bearing stresses from the rib. Overall, the cumulative effect of ring tension and compression strut allows the transfer of stresses from shear spring to the entire section of concrete due to the irregular shape of voronoi mesh. So, the entire cross-section of concrete could provide an optimum contribution towards equilibrium with shear stresses from beam element and the bond behavior could be evaluated in comparison to experiments.

5. Capability to Simulate Bond Mechanism of Cover Thickness and Rebar Diameter

5.1. Cover Thickness

In the previous section, the ability of voronoi mesh of 3D-RBSM to contribute towards the conical stress distribution mechanism has been mainly highlighted. However, it is yet to be understood how the proposed technique has inherited the ability to express the effect of variation in cover thickness on variation in bond stress slip behavior. To understand the mechanism, the internal stress distribution is discussed for the cover thickness cases, whose bond stress slip relationships were shown in Figs. 13, 17 and 23. Figs. 26 and 27 present the internal stress distribution in the direction of rebar. In Fig. 26, the stress distribution is shown at a section parallel to the rebar. While in Fig. 27, the internal stress distribution is shown at the section perpendicular to the rebar at a distance of 25mm from the top-loading end. The section at 25mm is selected to clearly observe the compression stress due to the inclined cracks from rebar to shear stress transfer. The stress distribution is given at slip values of 0.01 and 0.1mm in the pre-peak stage, at ultimate bond stress points, and 0.30mm slip in the post-peak stage. Considering bond stress slip relationships, bond stresses are almost the same for all cover thickness cases at 0.01mm slip. However, at 0.1mm slip, a 10mm cover thickness case shows smaller bond stress values than 30 and 50mm cover thickness cases. The progressive bond stress slip region shows a clear effect of cover thickness on bond behavior.

At a lower slip value of 0.01mm, tensile stress for a 10mm cover thickness case has reached to the specimen surface. However, concrete stress magnitude and area (tension and compression stresses) are almost the same for each cover thickness case, so bond stresses are also the same. With slip progressing in the non-linear stage, the net concrete stress magnitude varies dependent upon cover thickness. At 0.1mm slip, the region of tensile stresses is least for 10mm cover case, because tensile stresses slightly diminished at the minimum cover thickness side due to earlier progression of tensile stresses to the specimen surface. While, for 30 and 50mm cover case, the magnitude of concrete stresses is quite similar, so the bond stresses are similar.

At ultimate bond stress stages, a clear-cut effect of variation in cover thickness on variation in concrete stress distribution can be seen. Tensile (ring tension) and compressive stresses (compression struts) distribute to a wider region with an increase in cover thickness, therefore, the ultimate bond stresses increase.

Furthermore, the effect of variation in cover thickness is observed on stress distribution in the post-peak region. The findings reveal that the proposed simplified model is a realistic representation of experimentally observed bond mechanism under cover thickness effect.

5.2. Rebar Diameter

Several one-end and two-end pullout based experimental studies have outlined the influence of rebar diameter on bond behavior and various bond stress equations [11, 20 and 23] with an inverse function of rebar diameter have been formulated. This fact emphasizes that bond stresses decrease with an increase in rebar diameter. The proposed model does not utilize the rebar diameter as a function in the bond stress slip constitutive equation for the sake of simplicity. Also, the beam model is not a physical representation of rebar cross-section. Moreover, the distance of the beam element from the concrete surface is dependent upon the summation of real cover thickness and rebar radius, since the position of beam element is set at the center of rebar. As a representation of the effect of rebar diameter on bond behavior is an important aspect of an analytical model. So, to validate the applicability of the proposed model to simulate the rebar diameter effect, three rebar diameter cases of 19.1, 25.4 and 31.8mm are selected from the test results of Iizuka et al. [20]. The concrete strength of each specimen is 26.0, 25.1 and 21.2MPa, respectively. For all cases, the cover thickness is 30mm and mesh size is 10mm.

Fig. 28 shows the analytical effect of rebar diameter on bond stress slip behavior with experimental results. The analytical model evaluates that ultimate bond stresses, as well as the slip at ultimate bond stresses, decrease with an increase in rebar diameter. Furthermore, the proposed analytical model also shows the effect of variation in rebar diameter on change in stiffness of the bond stress slip curve, whereas the stiffness gradually decreases with an increase in rebar diameter. The experimental outcomes on rebar diameter variation are well simulated by the proposed model. To discuss the load resistance mechanism under equilibrium condition, the bond force slip relationship is more important than the bond stress slip relationship because bond stress depends on rebar diameter. Fig. 29 shows the bond force slip relationship for test and simulation. Bond force is obtained by multiplying bond stresses to the circumferential area of half embedment length of rebar. Fig. 29 reveals that analytically observed bond force slip tendency remains approximately similar in the pre-peak stage despite the different rebar diameter.

To discuss the mechanism of rebar diameter related to bond behavior, Figs. 30 and 31 show the internal stress distribution parallel to the rebar at section parallel and perpendicular to rebar at a distance of 25mm from the top-loading end, respectively. The stress distribution is shown in the pre-peak stage at 0.05 and 0.1mm slip, at ultimate bond stress points and in the post-peak stage at 0.3mm slip. Slip levels at the ultimate bond stress stage are 0.2, 0.12 and 0.13mm for 19.1, 25.4 and 31.8mm rebar diameter, respectively.

For the same cover thickness, the area for stress resistance is almost the same for different rebar diameter cases. Figs. 30 and 31 reveal that the magnitude of ring tension and compression struts is almost similar for different rebar diameter cases at the same slip levels in the pre-peak stage. Also, at the ultimate bond stress stage, the effect of different rebar diameter on stress distribution is almost similar. So, the bond force slip has almost similar behavior with different rebar diameters. On the other hand, bond stresses are normalized by circumferential area dependent upon rebar diameter, so bond stresses decrease with an increase in rebar diameter. In the post-peak stage at 0.30mm slip, slight variation in tension stress region can be observed with different rebar diameter cases. The variation is dependent upon the propagation of split cracks. Overall, the proposed analytical method can simulate the effect of rebar diameter on bond behavior leading to a reliable evaluation of a wide range of structures.

6. Conclusion

Based upon the outcomes of the proposed numerical method to model concrete by using voronoi mesh with random geometry and rebar by beam element combined with simplified local nonlinear bond stress slip model, the following conclusions are drawn:

1. The proposed numerical model can automatically simulate the effect of cover thickness on bond stress slip relationship and cracking behavior around rebar such as Goto cracks. So, the complicated parametric functional dependency of bond on cover thickness like FEM is not required to be modeled.

2. CEB-Shima hybrid local bond model is a suitable local bond stress slip model to be combined with the proposed method. The features are that initial stiffness is similar to the Shima model, while final stiffness and ultimate bond stress are similar to the CEB-FIP model. The model tends to evaluate the transition of failure modes along with the better evaluation of experimental results as compared to all former models.

3. The proposed methodology using a simple beam element for rebar modeling can simulate bond behavior like a mesoscale based 3D rebar model with rib shape. The merits of the proposed model are to reduce element numbers and computational time and freely arrange the reinforcing bars in the specimen domain rendering ease to the user.

4. The use of voronoi mesh is essential towards the propagation of conical cracks from the rib surface of deformed rebar promoting the ring tension phenomena observed in RC structures. The simulation by regular mesh modeling cannot evaluate the effect of cover thickness on bond behavior without introducing dimensional parameters in local bond stress slip relationship.

5. The model can evaluate the effect of variation in rebar diameter and cover thickness on bond behavior in accompany with the reasonable stress transfer mechanism.

6. It was confirmed that the proposed model is a good numerical substitute for mesoscale based 3D rebar model with rib shape and promotes efficient and economical aspects for application to a wide range of structural members.

7. The formation of a better analytical model to simulate post-peak behavior is a future target of this study.

Acknowledgment

This research presented in this work was conducted at Nagoya University.

References

1. D.A. Abrams, Test of bond between concrete and steel, Bulletin No. 71, University of Illinois XI (15), 1913.
2. L.A. Lutz, P. Gergely, Mechanics of bond and slip of deformed bars in concrete, ACI J. (1967) 711-721.
3. R. Tepfers, Cracking of concrete cover along anchored deformed reinforcing bars, Mag. Concr. Res. 31 (106) (1979) 3-12.
4. Y.L. Xu, Experimental study of anchorage properties for deformed bars in concrete, Ph.D. Thesis, Department of Civil Engineering, Tsinghua University, Beijing, China, 1990 [in Chinese].
5. B.B. Broms, Crack width and average crack spacing in reinforced concrete members, ACI J. 62 (10) (1965) 1237-1256.
6. Y. Goto, Cracks formed in concrete around deformed tension bars, ACI J. 68 (4) (1971) 244-251.
7. R.G. Mathey, D. Watstein, Investigation of bond in beam and pull-out specimens with high-yield-strength deformed bars, ACI J. 62 (1961) 1071-1090.
8. P.M. Ferguson, Bond stress: the state of art report by ACI committee 408, ACI Struct. J. 63 (11) (1966) 1161-1190.
9. S.M. Mirza, J. Houde, Study of bond stress-slip relationships in reinforced concrete, ACI Struct. J. 76 (2) (1979) 19-46.
10. E.L. Kemp, W.J. Wilhelm, Investigation of the parameters influencing bond cracking, ACI J. 76 (1) (1979) 47-71.
11. R. Eligehausen, E. P. Popov, V.V. Bertero, Local bond stress-slip relationships of deformed bars under generalized excitations, in: 7th European Conference on Earthquake Engineering, 1982, 69-80.

12. H. Shima, L. Chou, H. Okamura, Micro and macro models for bond in reinforced concrete, J. Faculty Eng., The University of Tokyo (B), XXXIX (2), 1987, 133-194.
13. P.S. Chana, A test method to establish realistic bond stresses, Mag. Concr. Res. 42 (151) (1990) 83-90.
14. R. Eligehausen, G.L. Balazs, Bond and detailing, in: Proceedings of the colloquium on the CEB-FIP MC90, Rio de Janeiro; 1991, 213-261.
15. D. Darwin, S.L. McCabe, E.K. Idun, S.P. Schoenekase, Development length criteria: bars not confined by transverse reinforcement, ACI Struct. J. 89 (6) (1992) 709-720.
16. A.J. Bigaj, Bond behaviour of deformed bars in NSC and HSC-experimental study, Report No. 25.5-95-11, Steven Laboratory, Faculty of Civil Engineering, Delft University of Technology, 1995.
17. M.H. Harajli, M. Hout, W. Jalkh, Local bond stress-slip behavior of reinforcing bars embedded in plain and fiber concrete, ACI Mater. J. 92 (4) (1995) 343-353.
18. M.H. Harajli, B.S. Hamad, A.A. Rteil, Effect of confinement of bond strength between steel bars and concrete, ACI Struct. J. 101 (5) (2004) 595-603.
19. M.H. Harajli, Bond stress–slip model for steel bars in unconfined or steel, FRC, or FRP confined concrete under cyclic loading, ASCE J. Struct. Eng. 135 (2009) 509-518.
20. K. Iizuka, T. Higai, S. Saito, R. Takahashi, Bond stress-slip-strain relationship of deformed bars including the effect of concrete cover thickness, J. JSCE 67 (2011) 280-296 [in Japanese].
21. Y.X. Zhao, H.W. Lin, K. Wu, W.L. Jin, Bond behaviour of normal/recycled concrete and corroded steel bars, Constr. Build. Mater. 48 (2013) 348-359.
22. H.W. Lin, Y. Zhao, J. Ozbolt, P. Feng, C. Jiang, R. Eligehasuen, Analytical model for the bond stress-slip relationship of deformed steel bars, Constr. Build. Mater. 198 (2019) 570-586.
23. CEB-FIP, Model Code 2010, First complete draft, vol. 1, Comité Euro-International du Béton, Lausanne, Switzerland, 2010.
24. JSCE, Standard specifications for structures-2012, Design, Japan Society of Civil Engineers, Japan 2012.

25. ACI Committee, 318 building code requirements for structural concrete and commentary 318-19, American Concrete Institute, Farmington Hills, MI, USA, 2019.
26. Z. Huang, A.M. ASCE, I.W. Burgess, R.J. Plank, Modeling membrane action of concrete slabs in composite buildings in fire. I: Theoretical Development, ASCE J. Struct. Eng. 129 (2003) 1093-1102.
27. A. Werner, Finite element modeling of large deformation response of reinforced concrete beams, Master Thesis, Department of Civil and Environmental Engineering, Northeastern University, Boston, MA, America, 2008.
28. R.C.G. Menin, L.M. Trautwein, T.N. Bittencourt, Smeared crack models for reinforced concrete beams by finite element method, Ibracon Struct. Mater. J. 2 (2) (2009) 166–200.
29. L. Jendele, J. Cervenka, Finite element modelling of reinforcement with bond, Comput. Struct. 84 (2006) 1780-1791.
30. D. Ngo and A.C. Scordelis, Finite element analysis of reinforced concrete beams, ACI J. 64 (1967) 152-163.
31. Y. Gan, Bond stress and slip modeling in nonlinear finite element analysis of reinforced concrete structures, Master thesis, Graduate Department of Civil Engineering, University of Toronto, Toronto (2000) 269.
32. L.N. Lowes, J.P. Moehle, S. Govindjee, Concrete-steel bond model for use in finite element modeling of reinforced concrete structures, ACI. Struct. J. 101 (4) (2004) 501-511.
33. H.M. Salem, K. Maekawa, Pre- and postyield finite element method simulation of bond of ribbed reinforcing bars, J. of Struct. Eng. 130 (4) (2004) 671–680.
34. M. Kurumutani, H. Anzo, K. Kobayashi, S. Okazaki, S. Hirose, Damage model for simulating chloride concentration in reinforced concrete with internal cracks, Cem. Concr. Compos. 84 (2017) 62-73.
35. L. Eddy, K. Nagai, Numerical simulation of beam-column knee joints with mechanical anchorages by 3D rigid body spring model, Eng. Struct. 126 (2016) 547-558.
36. K. Ikuma, Y. Yamamoto, H. Nakamura, T. Miura, Mesoscale simulation of bond behavior of deformed rebar based on coupled RBSM-FEM method, Proc. Japan Concr. Inst. 40 (2018) 541-546 [in Japanese].

37. Y. Yamamoto, H. Nakamura, I. Kuroda, N. Furuya, Analysis of compression failure of concrete by three dimensional rigid body spring model, JSCE Proceedings, 64 (4) (2008) 612-630 [in Japanese].
38. Y. Yamamoto, H. Nakamura, I. Kuroda, N. Furuya, Crack propagation analysis of reinforced concrete wall under cyclic loading using RBSM, Euro. J. Environ. Civ. Eng. 18 (2014) 780-792.
39. J.E. Bolander, G.S. Hong, Rigid-body-spring network modeling of prestressed concrete members, ACI Struct. J. 99 (5) (2002) 595-604.
40. Y.H. Gedik, H. Nakamura, Y. Yamamoto, M. Kunieda, Evaluation of three-dimensional effects in short deep beams using a rigid-body-spring-model, Cem. Concr. Compos. 33 (2011) 978-991.
41. H. Nakamura, T. Iwamoto, L. Fu, Y. Yamamoto, T. Miura, Y.H. Gedik, Shear resistance mechanism evaluation of RC beams based on arch and beam actions, J. Adv. Concr. Tech. 16 (2018) 563-576.
42. U. Farooq, H. Nakamura, Y. Yoshihito, T. Miura, Evaluation of cracking and deformation behavior of RC beams reinforced with high strength rebar, Proc. Japan Concr. Inst. 40 (2018) 139-144.
43. K.K. Tran, H. Nakamura, K. Kawamura, M. Kunieda, Analysis of crack propagation due to rebar corrosion using RBSM, Cem. Concr. Compos. 33 (2011) 906-917.
44. D. Qiao, H. Nakamura, Y. Yamamoto, T. Miura, Crack patterns of concrete with a single rebar subjected to non-uniform and localized corrosion, Constr. Build. Mater. 116 (2016) 366-377.
45. Y. Yang, H. Nakamura, T. Miura, Y. Yamamoto, Effect of corrosion-induced crack and corroded rebar shape on bond behavior, Struct. Concr. (2019) 1-12.
46. M. Suga, H. Nakamura, T. Higai, S. Saito, Effect of bond properties on the mechanical behavior of RC beam, Proc. Japan Concr. Inst., 23 (3) (2001) 295-300 [in Japanese].

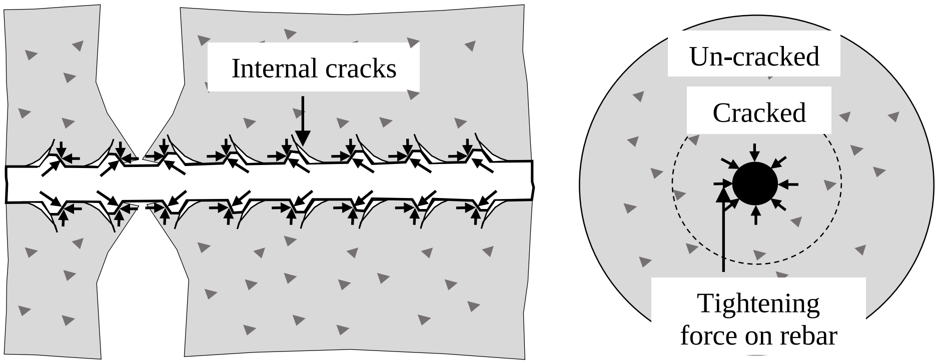

Fig. 1 Internal cracks around deformed rebar [5].

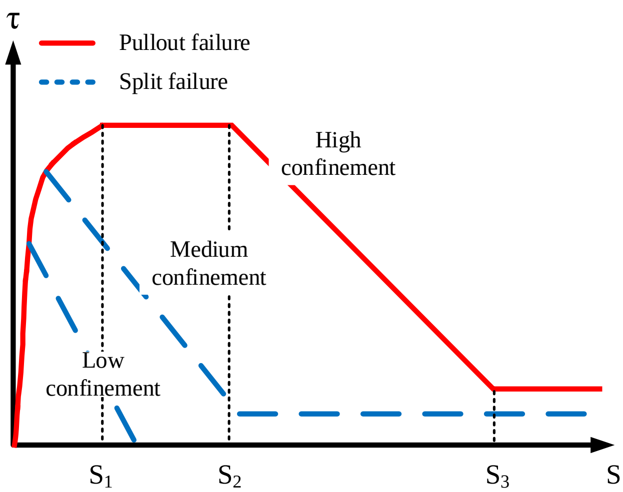

Fig. 2 Influence of confinement on bond behavior [23].

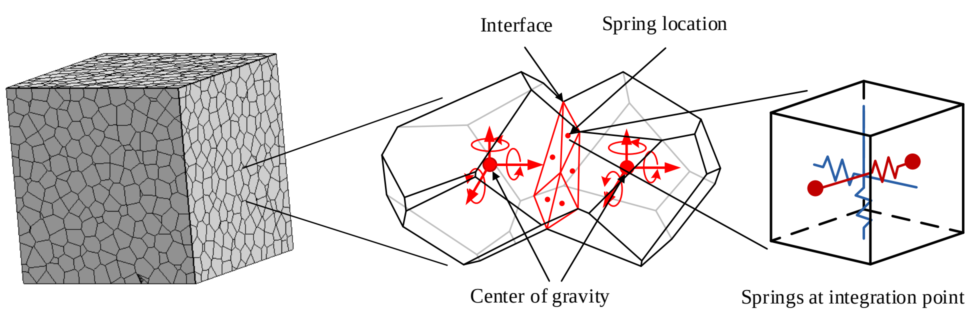

Fig. 3 Concrete model.

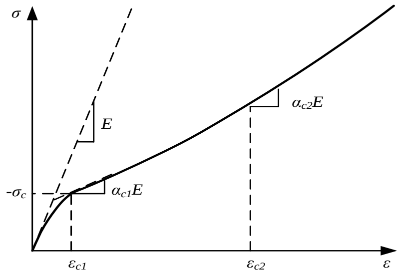

Fig. 4 Compression model of normal spring.

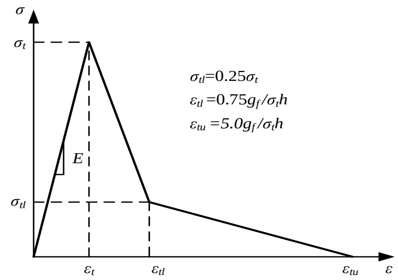

Fig. 5 Tension model of normal spring.

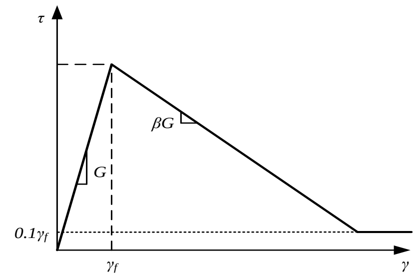

Fig. 6 Shear spring model.

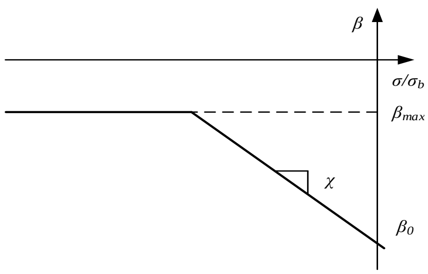

Fig. 7 Softening coefficient for shear spring.

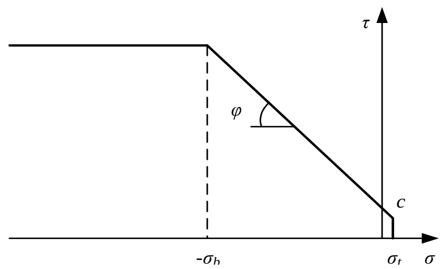

Fig. 8 Mohr-coulomb criteria.

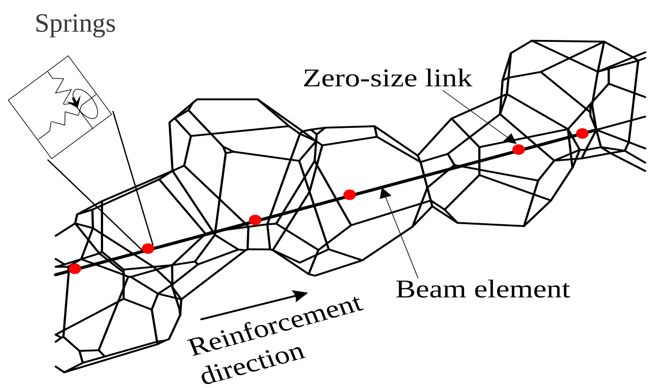

Fig. 9 Beam element based reinforcement model.

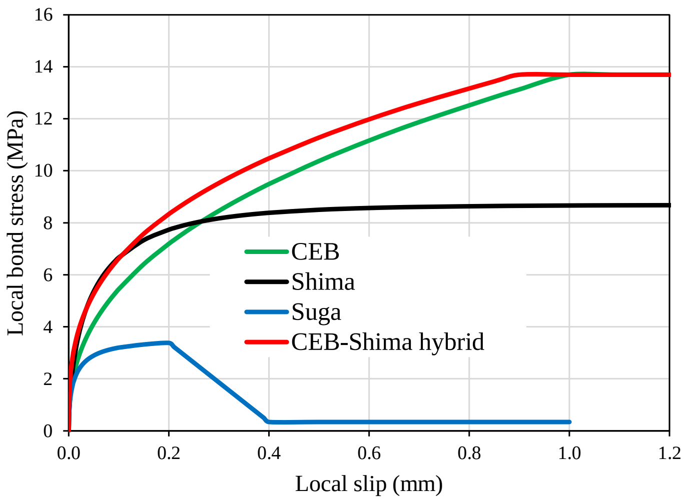

Fig. 10 Various local bond stress-slip models.

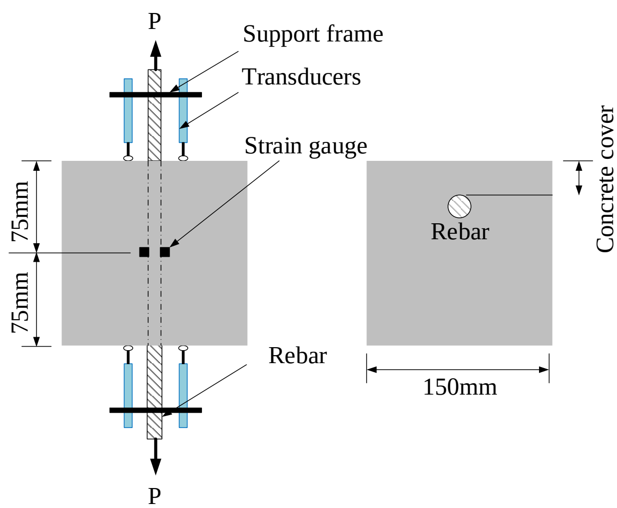

Fig. 11 Schematic diagram of two-end pullout test conducted by Iizuka et al. [20].

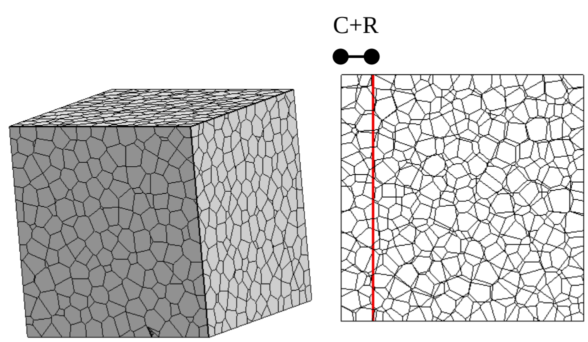

Fig. 12 Numerical model of two-end pullout test (Mesh Size: 10mm).

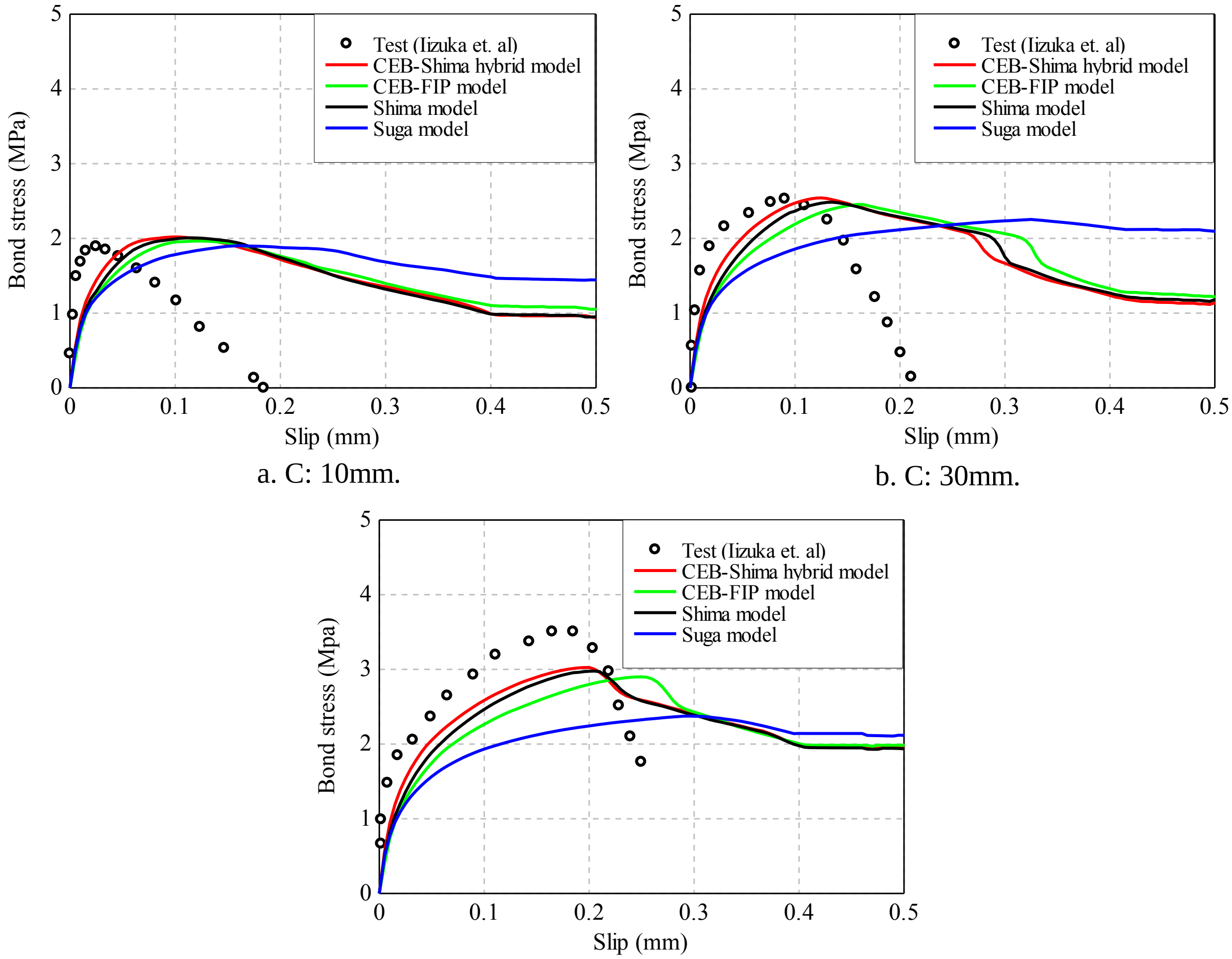

a. C: 10mm.

b. C: 30mm.

c. C: 50mm.

Fig. 13 Influence of local bond model on bond behavior.

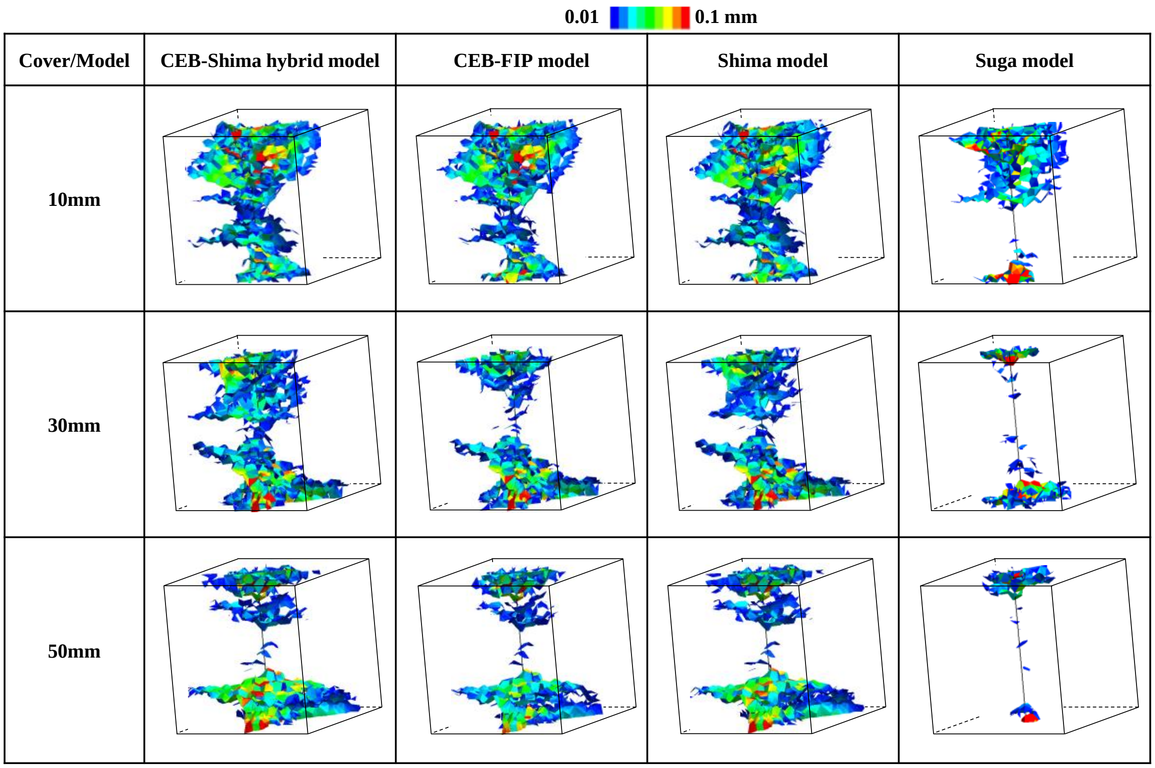

Fig. 14 Analytically observed internal crack distribution at 0.30mm slip. Column: Different local bond models. Rows: Different cover thickness specimens. Blue color: Minimum crack width of 0.01mm. Red color: Crack width equal or greater than 0.1mm.

Cover/Model	CEB-Shima hybrid model	CEB-FIP model	Shima model	Suga model
10mm	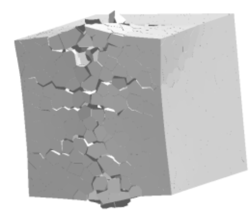	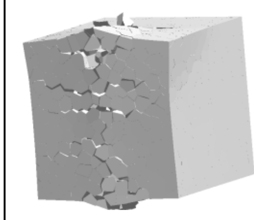	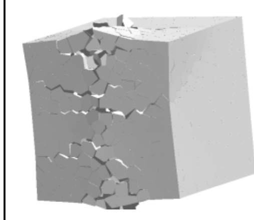	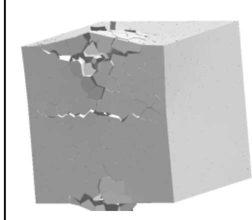
30mm	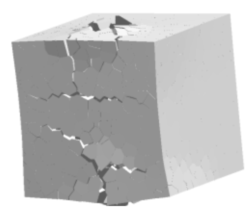	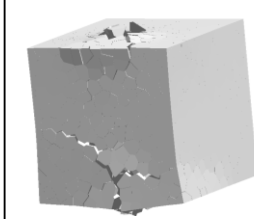	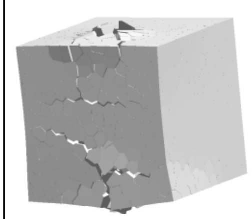	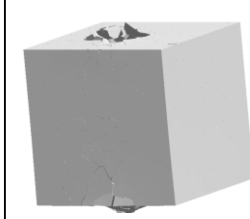
50mm	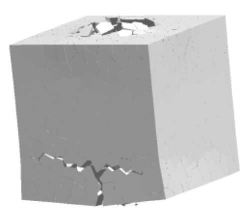	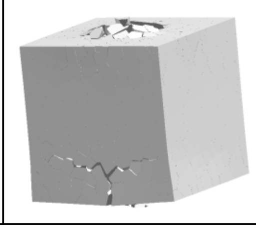	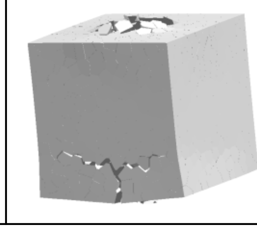	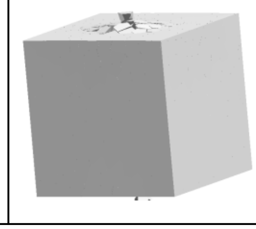

Fig. 15 Analytically observed deformation behavior at 0.30mm slip. Columns: Different local bond models. Rows: Different cover thickness specimens. Magnification: 50 times.

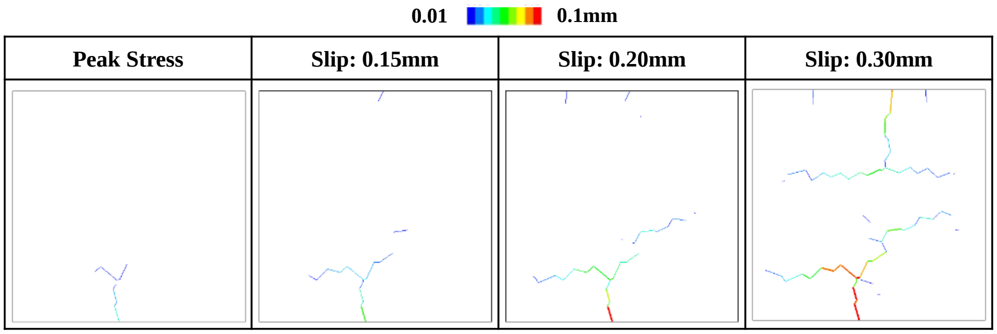

Fig. 16 Analytically observed failure process, with CEB-Shima hybrid bond model for 30mm cover thickness specimen, at the surface near to the minimum cover thickness. Blue color: Minimum crack width of 0.01mm. Red color: Crack width equal or greater than 0.1mm.

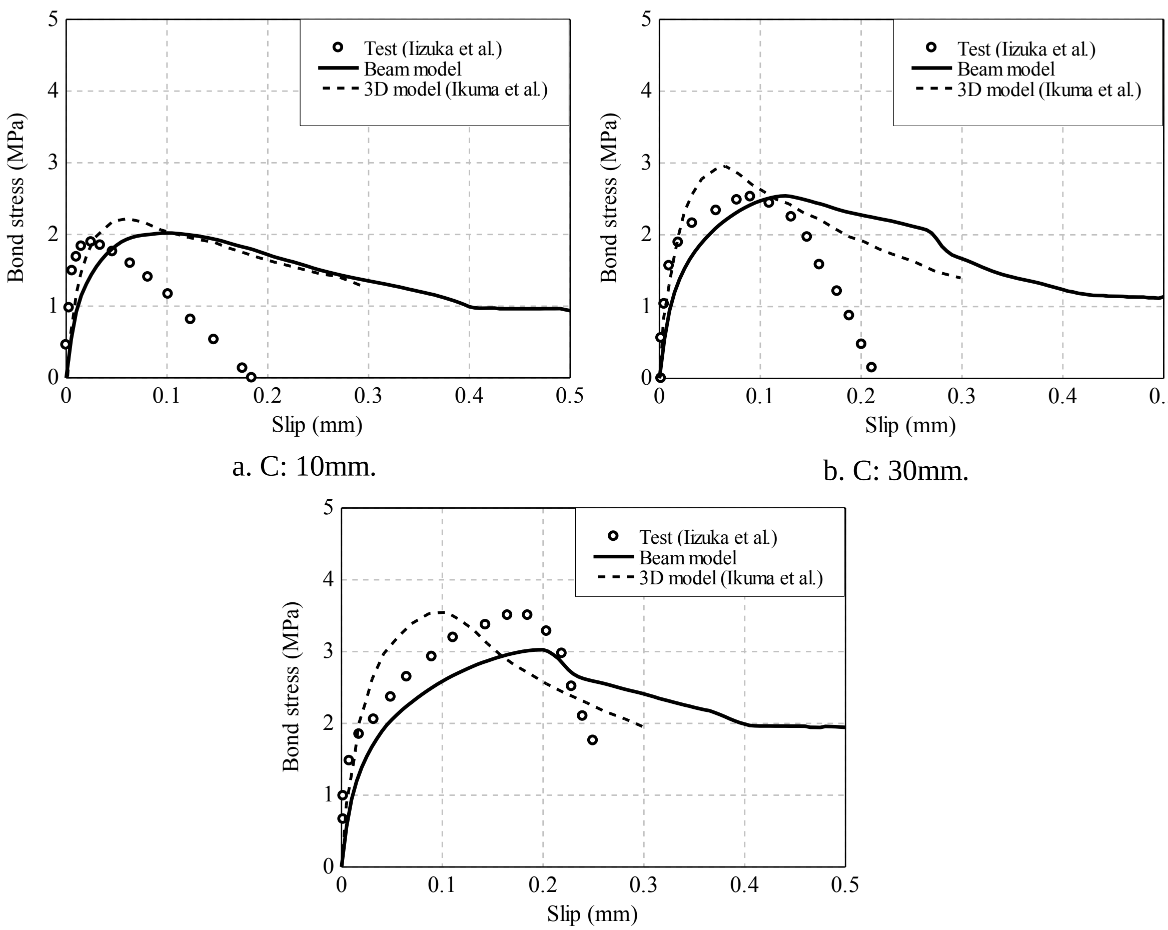

a. C: 10mm.

b. C: 30mm.

c. C: 50mm.

Fig. 17 Evaluation of various reinforcement models, used in analytical methods, to simulate bond behavior. Beam model is used in present study. 3D model is used by Ikuma et al. [36].

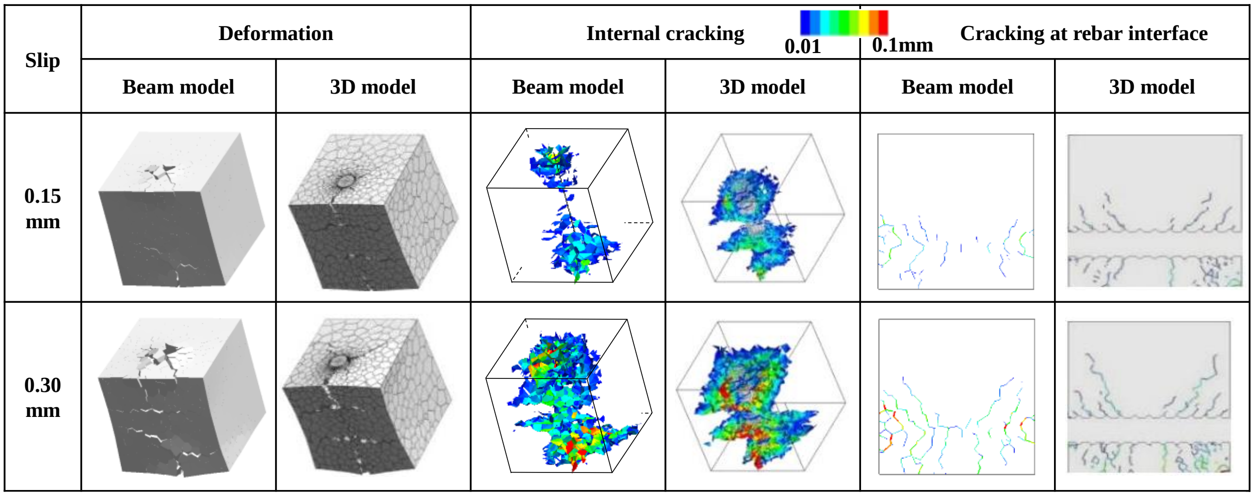

Fig. 18 Cracking behavior comparison between beam element and 3D rebar model for 30mm cover thickness specimen. Columns 2, 4 and 6: Deformation, internal cracking and cracking at rebar interface, respectively, observed by using beam model in present study. Columns 3, 5 and 7: Deformation, internal cracking and cracking at rebar interface, respectively, observed by Ikuma et al. [36] by using 3D model. Rows: Different slip levels. Blue color: Minimum crack width of 0.01mm. Red color: Crack width equal or greater than 0.1mm. Magnification: 50 times.

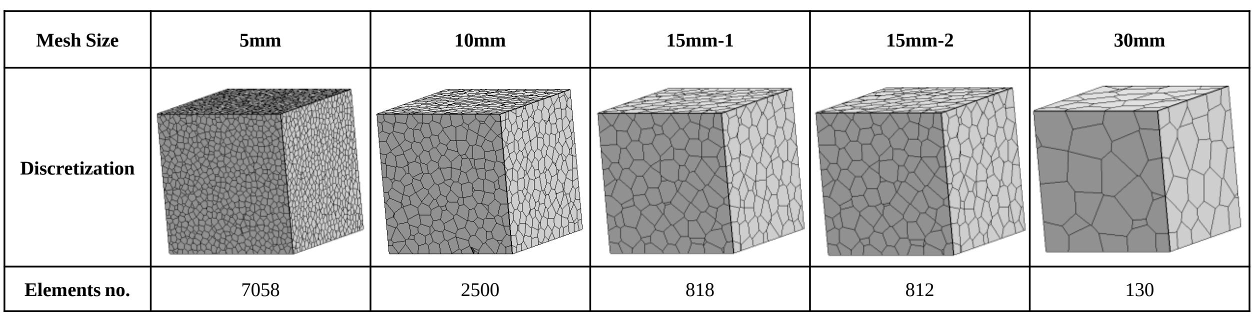

Fig. 19 Voronoi mesh arrangement with different mesh sizes and mesh discretization. 15mm mesh discretized as 15mm-1 and 15mm-2.

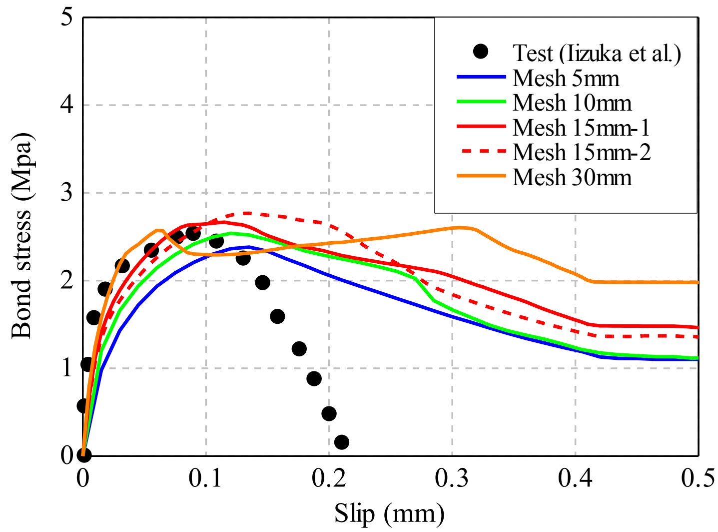

Fig. 20 Influence of mesh size and mesh discretization on bond stress slip behavior for 30mm cover thickness specimen.

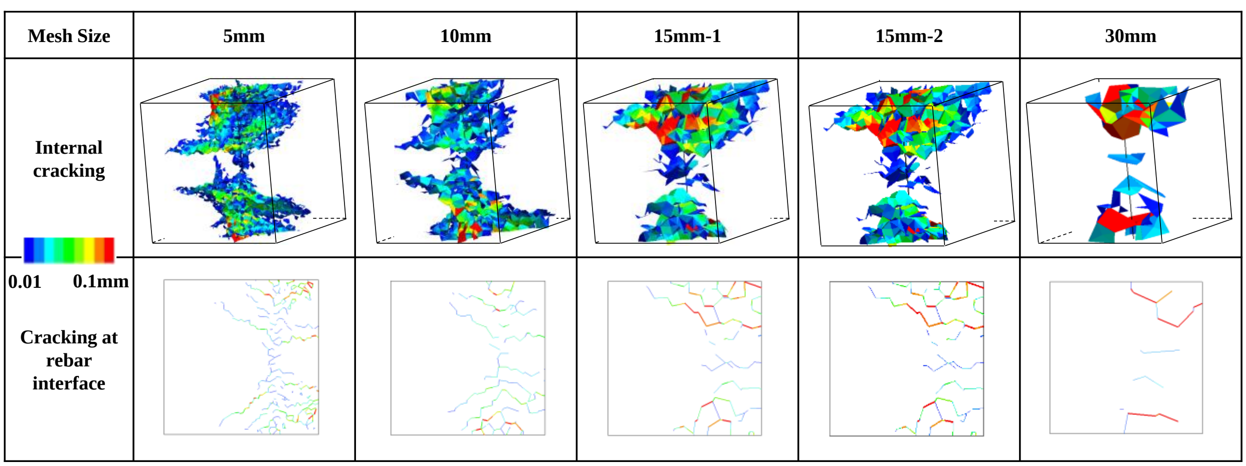

Fig. 21 Influence of mesh size and mesh discretization on crack propagation for 30mm cover thickness specimen at 0.30mm slip. Blue color: Minimum crack width of 0.01mm. Red color: Crack width equal or greater than 0.1mm.

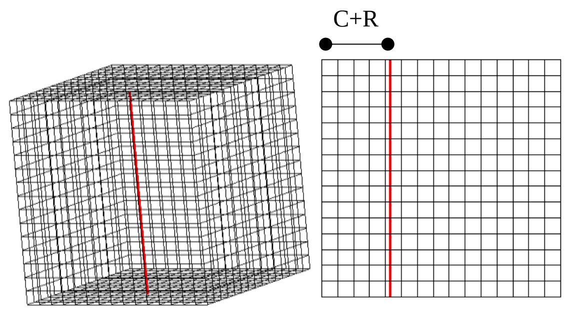

Fig. 22 Regular mesh shape model (Mesh size: 10mm)

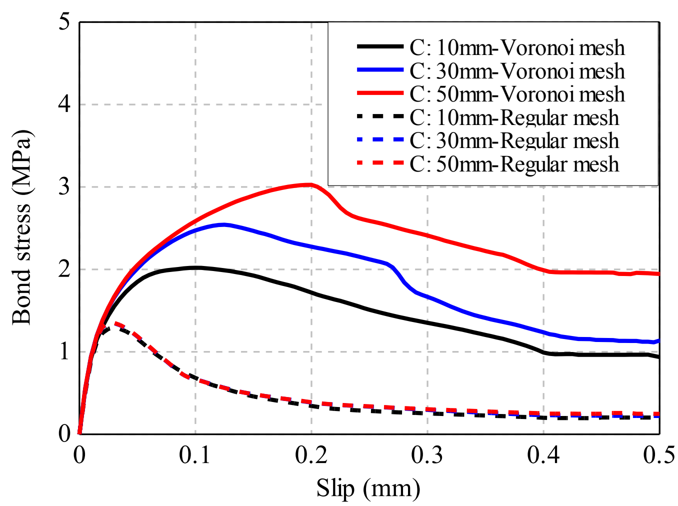

Fig. 23 Bond stress slip behavior comparison between regular and voronoi mesh for different cover thickness specimens. For both mesh cases, beam model is used.

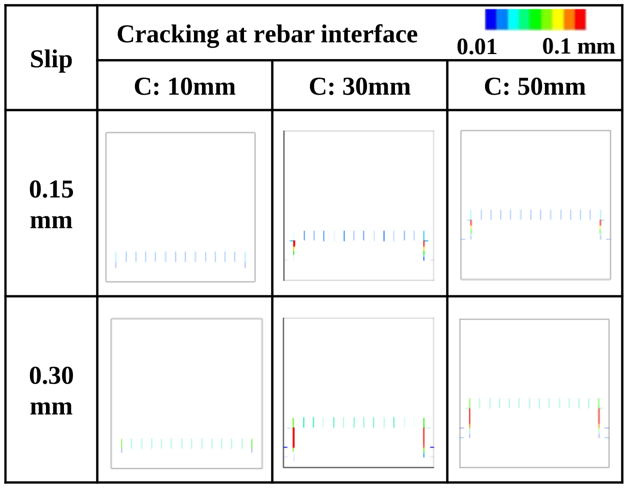

Fig. 24 Cracking at rebar interface for regular mesh with beam model. Columns: Different cover thickness specimens. Rows: Different slip levels. Blue color: Minimum crack width of 0.01mm. Red color: Crack width equal or greater than 0.1mm.

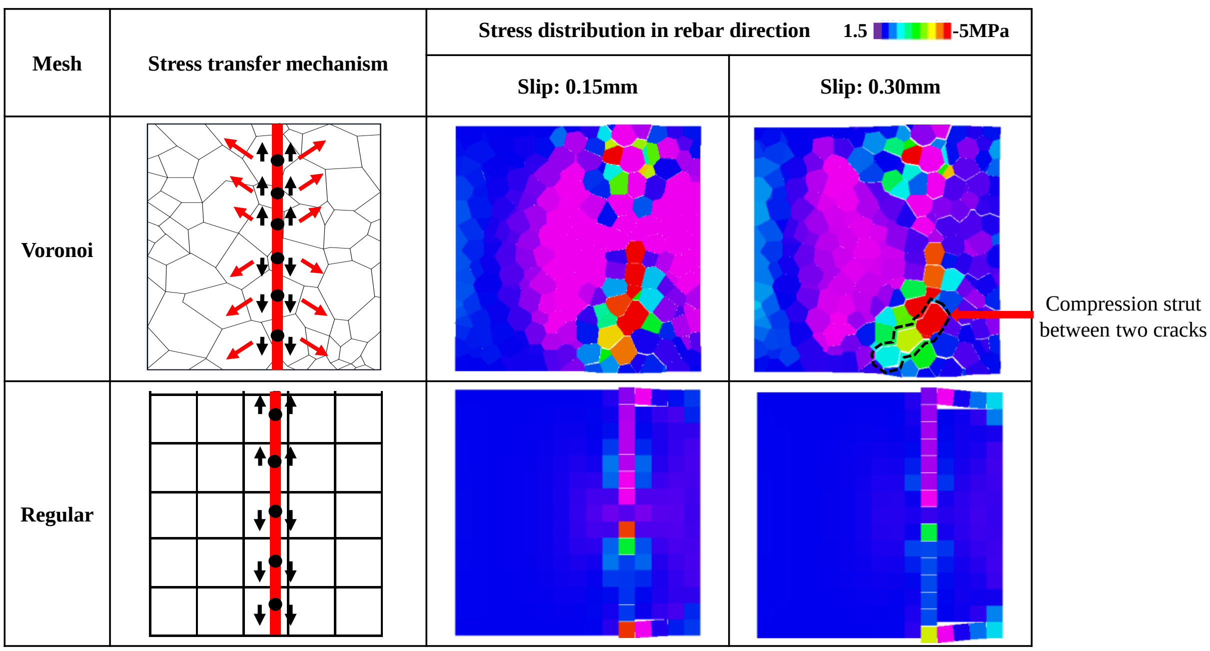

Fig. 25 Stress transfer mechanism and concrete stress distribution based on voronoi and regular mesh for 30mm cover thickness specimen at various slip levels. For both mesh cases, beam model is used. Bright purple color: Tension stress equal or greater than 1.5MPa. Blue color: Zero stress. Red color: Compression stress equal or greater than 5MPa.

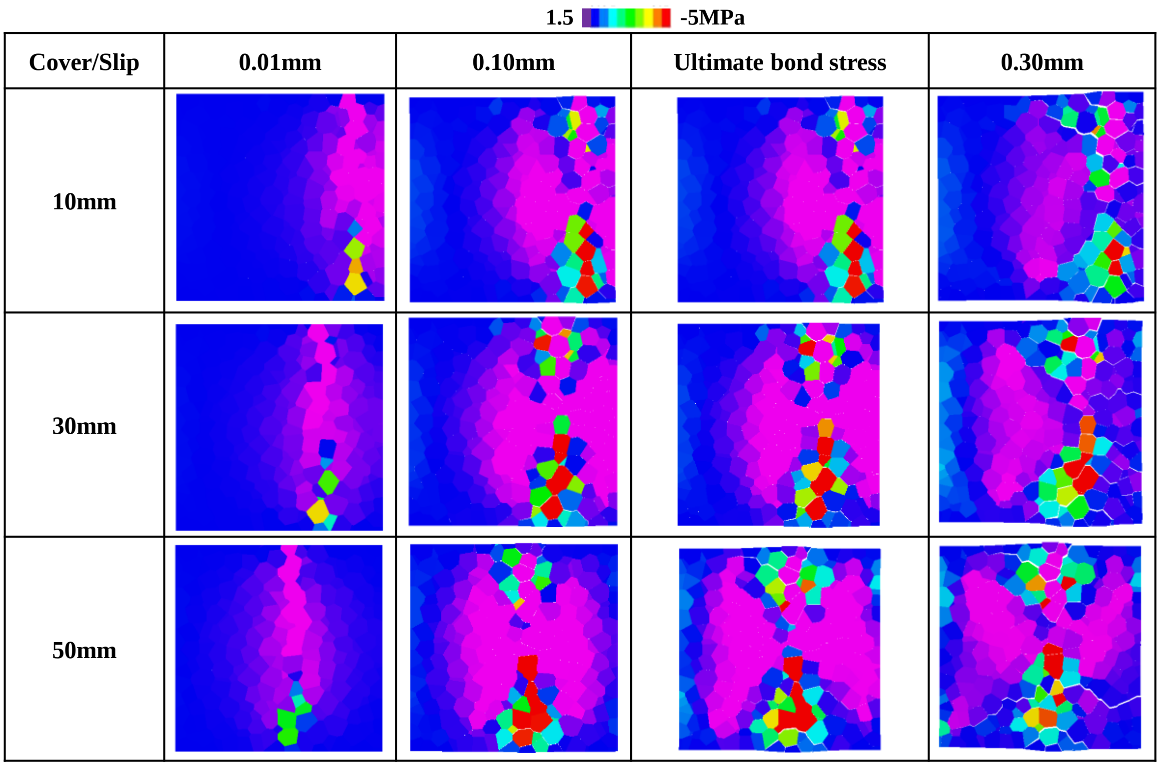

Fig. 26 Effect of change in cover thickness on stress distribution at section parallel to rebar including the rebar. Columns: Different slip levels including the ultimate bond stress stage. Rows: Different cover thickness specimens. Bright purple color: Tension stress equal or greater than 1.5MPa. Blue color: Zero stress. Red color: Compression stress equal or greater than 5MPa.

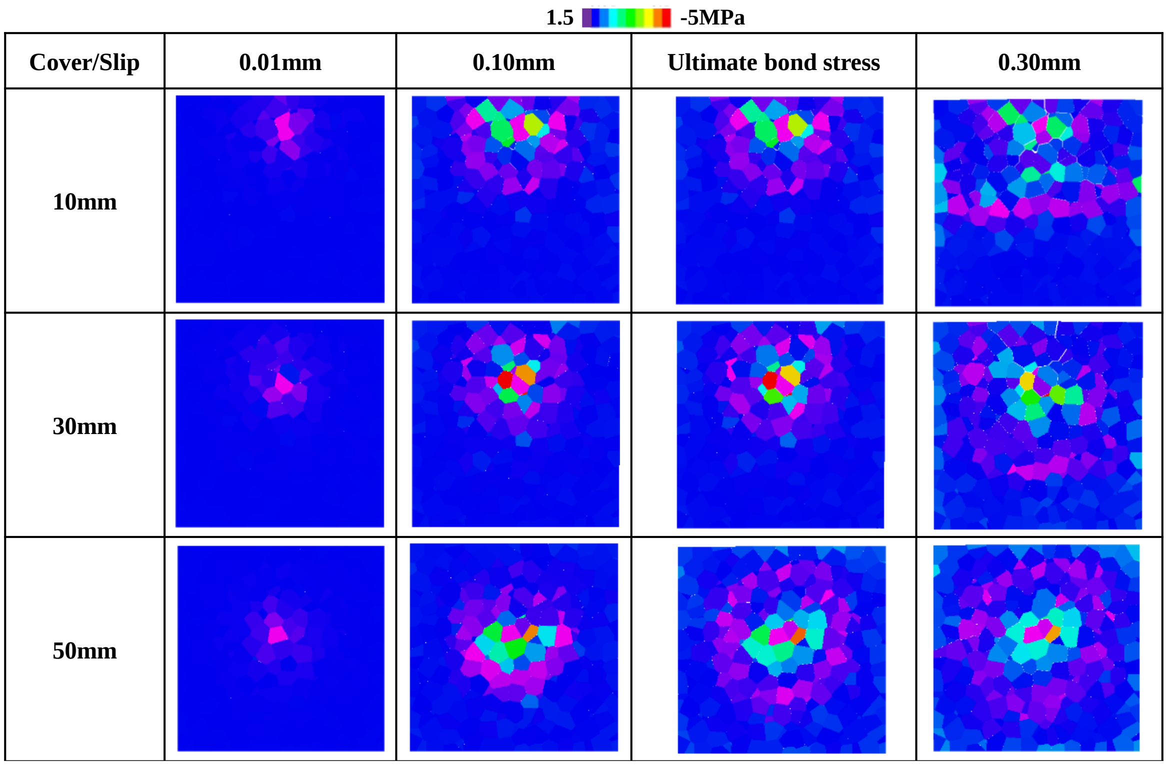

Fig. 27 Effect of change in cover thickness on stress distribution at section perpendicular to rebar at 25mm distance from top loading end. Columns: Different slip levels including the ultimate bond stress stage. Rows: Different cover thickness specimens. Bright purple color: Tension stress equal or greater than 1.5MPa. Blue color: Zero stress. Red color: Compression stress equal or greater than 5MPa.

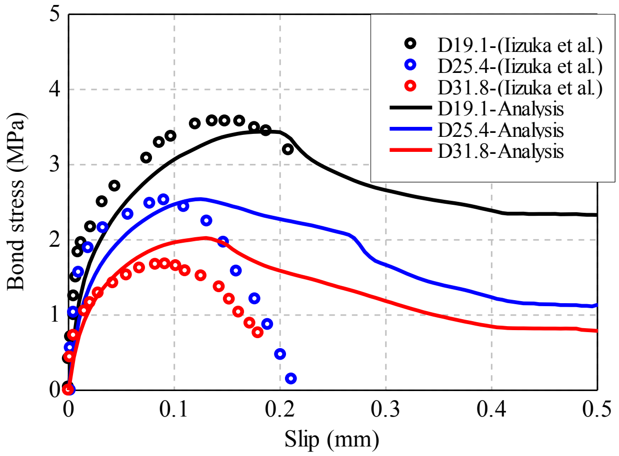

Fig. 28 Rebar diameter influence on bond stress slip behavior for 30mm cover thickness specimen.

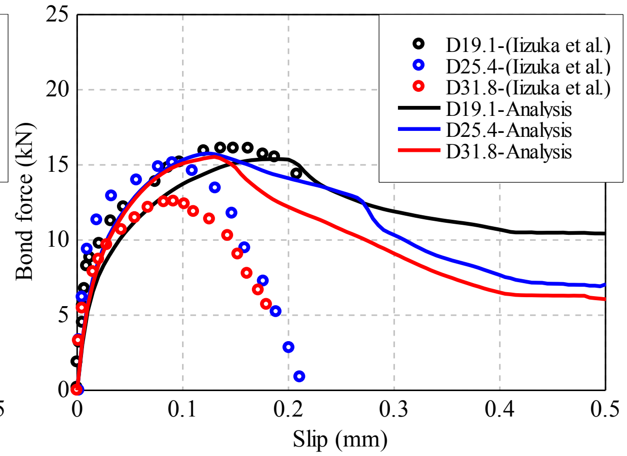

Fig. 29 Rebar diameter influence on bond force slip behavior for 30mm cover thickness specimen.

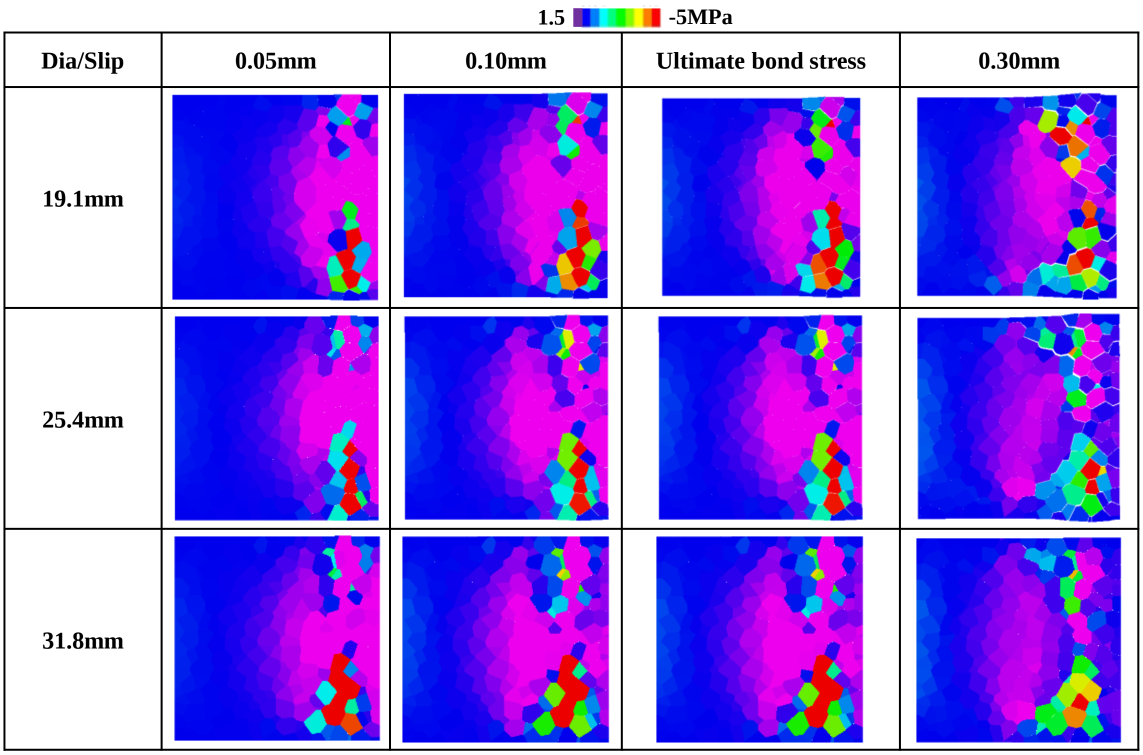

Fig. 30 Effect of change in cover thickness on stress distribution at section parallel to the rebar including the rebar for 30mm cover thickness specimen. Columns: Different slip levels including the ultimate bond stress stage. Rows: Different rebar diameter specimens. Bright purple color: Tension stress equal or greater than 1.5MPa. Blue color: Zero stress. Red color: Compression stress equal or greater than 5MPa.

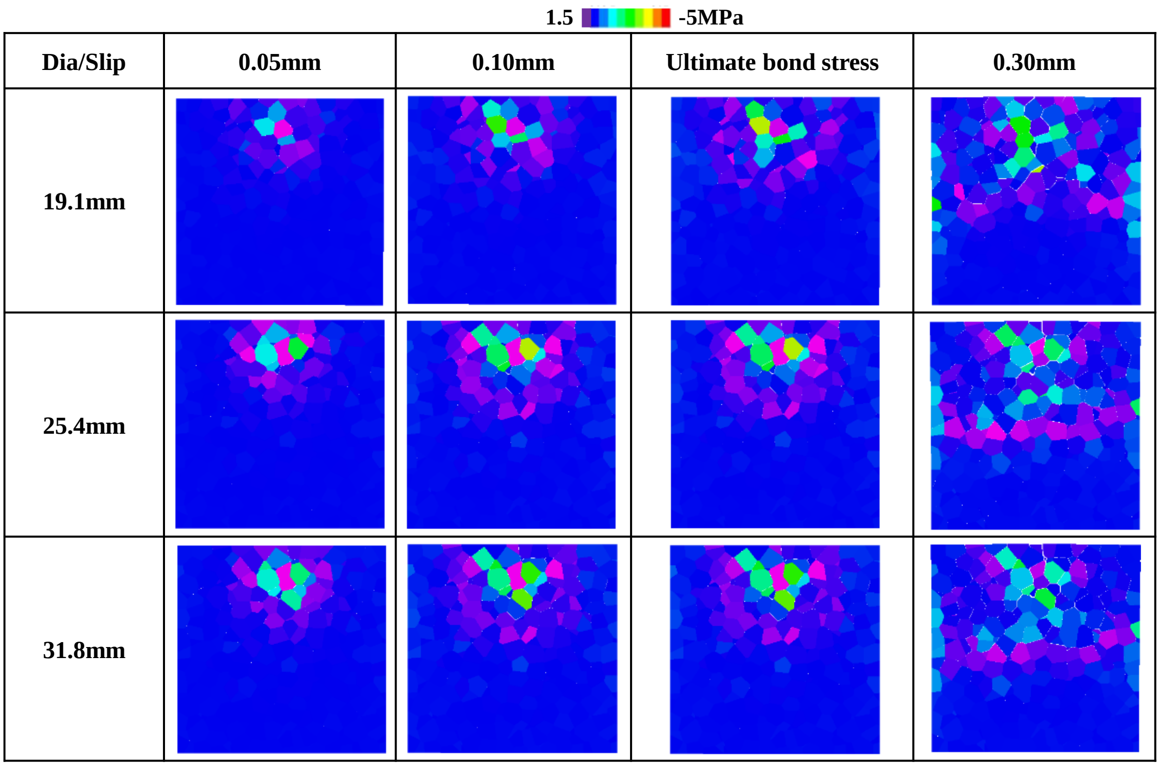

Fig. 31 Effect of change in cover thickness on stress distribution at section perpendicular to rebar at 25mm distance from top loading end for 30mm cover thickness specimen. Columns: Different slip levels including the ultimate bond stress stage. Rows: Different rebar diameter specimens. Bright purple color: Tension stress equal or greater than 1.5MPa. Blue color: Zero stress. Red color: Compression stress equal or greater than 5MPa.

137